RSC Advances




ROYAL SOCIETY OF CHEMISTRY

www.rsc.org/advances

Journal Name

ARTICLE

# Controlled Thermal Nitridation Resulting in Improved Structural and Photoelectrochemical Properties from $Ta_3N_5$ Nanotubular Photoanodes†

Received 00th January 20xx,
Accepted 00th January 20xx

DOI: 10.1039/x0xx00000x

www.rsc.org/

Sherdil Khan,[a] Sérgio Ribeiro Teixeira,[a] and Marcos Jose Leite Santos[b]*

$Ta_3N_5$ nanotubular photoanodes were synthesized by thermal nitridation of anodized $Ta_2O_5$ nanotubes (NTs) in a temperature range from 650°C to 1000°C. XRD diffractograms and Rietveld Refinements show that the crystalline structure is strongly dependent on thermal nitridation that triggers defects in the orthorhombic structure of $Ta_3N_5$ NTs. A non–stoichiometric $TaN_{0.1}$ phase was observed at the bottom of the $Ta_3N_5$ NTs at Ta–$Ta_3N_5$ interface. Electrochemical impedance spectroscopy revealed that nitridation conditions such as temperature and time strongly influence the interfacial charge transportation; affecting the photoelectrochemical (PEC) activities of the photoanodes. Improved PEC performance was obtained from the NTs synthesized at higher temperature for shorter nitridation time. This result is related to the preservation of the tubular morphology obtained at short nitridation time, high crystallinity and lower charge transfer resistance across the semiconductor–electrolyte interface.

## Introduction

In recent years, much more efforts have been devoted to the development of technologies to generate and store clean energy. The search for new materials is constantly growing and nano-structured semiconductors have been the focus of intensive study.[1,2,3,4] Tantalum nitride ($Ta_3N_5$) has received an increasing attention for application in water splitting, mainly due to its near optimal band structure.[5,6,7] $Ta_3N_5$ nanotubes (NTs) have been found to present an enormous potential for applications in photoelectrochemical (PEC) devices.[8,9,10] To synthesize $Ta_3N_5$ that presents tubular morphology at high temperature nitridation; the precursor ($Ta_2O_5$ NTs) should be synthesized in conditions that result in thick walled nanotubes with increased adherence to the Ta substrate.[11] For $Ta_3N_5$ presenting tubular morphology, a thorough investigations on lower and higher temperature nitridation at which pristine $Ta_3N_5$ with tubular morphology can be obtained and conditions at which they present improved crystallinity are warranted.

Electrochemical impedance spectroscopy (EIS) is a powerful tool to study the semiconductor–electrolyte interface. The equivalent circuit (EC) analogy simplifies the elucidation of electrochemical systems; provided the particular arrangement of circuit elements in a network possesses physical meaning.[12,13] Using EIS and EC to investigate the interfacial charge transportation of $Ta_3N_5$ NTs synthesized under different nitridation conditions are interesting to understand their PEC activity and to optimize them for improved performance.

In this work, we study the effect of nitridation temperature on the morphology, crystalline structure, interfacial charge transfer, PEC activity and flat band potential of $Ta_3N_5$ NTs. A detailed investigation is provided to study the $Ta_3N_5$ nanotubular electrodes prepared at i) increasing temperatures during short nitridation time, ii) increasing temperatures during long nitridation time and iii) fixed temperatures for varying nitridation time.

## Experimental

### $Ta_3N_5$ nanotubes preparation

$Ta_3N_5$ NTs were synthesized by nitridation of $Ta_2O_5$ NTs prepared by anodization.[14] The anodization was carried out employing a two electrode electrochemical configuration using Ta foil (Alfa Aesar, purity 99.95%) as anode and Cu disk as cathode. The electrolyte was a mixed solution of $H_2SO_4$ (Lab-Synth Products Laboratory LTD, 98.0%) + 1 vol% of HF and 4 vol% of distilled water. A DC voltage of 50 V was applied for 20 min by an initial ramping of 10 V/s at 10°C of the electrolyte temperature. Prior to nitridation, the as-anodized samples were etched in HF: $H_2O$ for few seconds, rinsed with water, dried under nitrogen flow, placed on an alumina boat and inserted into a horizontal quartz tube furnace. The heating and cooling rates of the furnace was maintained at 5°C/min under a 100 ml/min of constant gas flux consisting of a special mixture of ammonia: argon (1: 9 v/v). The pressure of the gas from the cylinder was fixed at 5

[a] Instituto de Física, UFRGS, Av Bento Gonçalves 9500 PO Box - 15051 91501-970, Porto Alegre-RS, Brazil. Phone: +55-51-33086498
[b] bInstituto de Química, UFRGS, Av Bento Gonçalves 9500 PO Box - 15051 91501-970, Porto Alegre, Brazil. Phone: +55-51-33089625
*Email: mjls@ufrgs.br
† Electronic Supplementary Information (ESI) available: [Figures and Tables]. See DOI: 10.1039/x0xx00000x

bar. Samples were obtained at nitridation temperature ranging from 650°C to 1000°C and nitridation times from 1 to 10 h. Three sets of samples have been synthesized: i) performing nitridation for 10 h at the temperatures of 650°C, 700°C, 750°C, 800°C and 900°C, ii) at constant nitridation temperature of 800°C during nitridation times of 1, 2, 3, 5 and 10 h and iii) performing nitridation for 3 h at the temperatures of 800°C, 850°C, 900°C and 1000°C. For simplicity, the samples are labeled as T°C-time, e.g. the sample nitrided at 800°C for 1 hour is represented as 800°C-1h.

**Characterizations**

Scanning electron microscopy (SEM) and transmission electron microscopy (TEM) were performed using EVO 50 from Zeiss operated at 10 kV and Jeol JEM 1200 EXII, respectively. SEM cross section images were obtained from samples scratched off the substrate. High resolution transmission electron microscopy (HRTEM) images were acquired using an XFEG Cs-corrected FEI Titan 80/300 microscope at INMETRO operated at 300 kV. XRD diffractograms of the $Ta_3N_5$ NTs adhere to the Ta substrate were obtained by using Rigaku Ultima IV diffractometer with Cu Kα radiation (λ = 1.54 Å) at a $2\vartheta$ range from 10° to 90° with a 0.05° step size and measuring time of 1s per step. Grazing angle XRD was recorded by Shimadzu, Maxima XRD-7000 diffractometer with an incident angle of 0.3° with Cu Kα radiation (λ = 1.54 Å) at a $2\vartheta$ range from 10° to 70° with a 0.05° step size and measuring time of 5 s per step. The XRD patterns were recorded under "Bragg-Brentano geometry". Data processing was performed by the Rietveld refinements using the same methodology as presented in our previous report.[5,11] UV-Vis diffuse reflectance was performed by using a CARY 5000. Contributions from scattering were removed by using Kubelka–Munk function and the bandgap energies were determined by finding the intercept of the straight line in the low energy region of a plot of $[K.M\ (R)hv]^{0.5}$ vs $hv$ for indirect and for $[K.M\ (R)hv]^2$ vs $hv$ for direct transition; $hv$ is the energy of the incident photons. X-ray photoelectron spectroscopy (XPS) was carried out at beamline SXS of the Brazilian Synchrotron Light Laboratory. The operating pressure in the ultrahigh vacuum chamber (UHV) during the analysis was $1 \times 10^{-9}$ Pa. The XPS spectra were collected using incident photon energy of 1840 eV. Energy steps were of 20 eV with 0.1 eV step energy and 200 ms per point acquisition time. The C 1s peak of adventitious carbon was fixed at 284.6 eV to set the binding energy scale.

**Photoelectrochemical characterization**

PEC measurements were performed using Auto-lab (AUT 84503) potentiostat. The experiments were performed in a quartz cell using standard three-electrode configuration employing the $Ta_3N_5$ NTs as working electrode, Pt wobbling electrode as counter electrode and Ag/AgCl as reference electrode. The electrolyte was 0.1 M $K_4[Fe(CN)_6]$ (Merck) and 0.1 mM $K_3[Fe(CN)_6]$ (Merck) at pH 7.5. Prior to each measurement the electrolyte was purged by argon gas and the $Ta_3N_5$ NTs photoanodes were cleaned by immersion in HF:$H_2O$ for few seconds and subsequently rinsed with distilled water and dried under nitrogen flow. During photocurrent-voltage measurements the working electrode was irradiated with a 300 W Xenon lamp. The polychromatic radiation was filtered by AM 1.5G–filter and the light intensity was calibrated to 100 mW.cm$^{-2}$ (1 sun) using a silicon photodiode. Hand light chopping LSV (linear sweep voltammetry) curves with a 5 sec periodic interval of light On and light Off were obtained at a scan rate of 10 mV/s. Nyquist plots were obtained at a frequency range of 100 kHz – 100 mHz with an amplitude of 5 mV. Mott-Schottky plots were obtained under a frequency of 500 Hz at 5 mV of amplitude for a range of the applied potentials. The measured potential versus the Ag/AgCl was converted to the RHE scale according to the following relation:

$$V_{RHE} = V_{Ag/AgCl} + (0.059) \times pH + 0.197\ V$$

Incident photon to electron conversion efficiency (IPCE) measurements were performed at 0 V vs Ag/AgCl using Oriel cornerstone monochromator.

## Results and discussion

**Morphology**

**Fig. 1** displays the SEM and TEM images of the samples synthesized by nitridation for 10 h at 650°C, 800°C and 900°C. One can observe an increase in roughness on the walls of the NTs with the temperature. However, upon thermal nitridation for 10 h at 900°C; a remarkable collapse in the tubular morphology is observed as the nanotubes are shrunk and turn into an urchin–like structure (**Fig. 1c**). As most of the literature on $Ta_3N_5$ describes the synthesis at 800°C, we have obtained nanotubes at this temperature and varied the nitridation times for; 1h, 2h, 3h, 5h and 10h.[9,15]

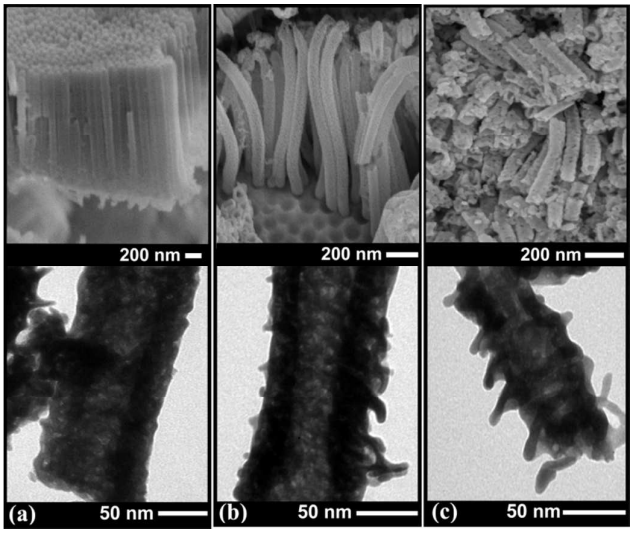


**Fig. 1** SEM (Top) and TEM (Bottom) images of the samples prepared for the nitridation time of 10h at (a) 650°C (b) 800°C and (c) 900°C.

**Fig. 2** compares the morphology of 800°C-5h and the samples prepared at 850°C, 900°C and 1000°C obtained for the nitridation time of 3h. As tubular morphology is observed for 800°-10h (**Fig. 1b**) and 800°C-5h (**Fig. 2a**); therefore, regardless of the nitridation time all the samples prepared at 800°C and samples that are 700°C-10h

and 750°C-10h have maintained their tubular morphology. Furthermore, it can be seen that the tubular morphology is only sustained at the temperature as high as 900°C (**Fig. 2d & 2e**), because at 1000°C (**Fig. 2c**) the nanotubes collapsed and the walls are cracked and periodic holes in the entire length are observed. The nitridation temperatures and times have changed the geometrical dimensions of the $Ta_3N_5$ NTs compared to the anodized NTs (**Table S1)** that is related to the density difference between $Ta_2O_5$ and $Ta_3N_5$.[16] The key to preserve the morphology of the $Ta_3N_5$ NTs for nitridation at higher temperatures lies in the low temperature anodization to prepare $Ta_2O_5$ NTs; resulting in strong adhesion to the Ta substrate and presenting thick walls.[11,14] The results show that for both conditions of long nitridation time of 10 h at 900°C (**Fig. 1c**) and for short periods of 3 h at 1000°C **(Fig. 2)** the nanotubes collapsed. Therefore, to preserve the tubular morphology low temperature anodization of the precursor is beneficial for sufficiently high nitridation temperature applied for short enough time. Furthermore, HRTEM image of the $Ta_3N_5$ NTs (**Fig. 2f**) viewed along [1-10] zone axis displays the interplanar distances of 5.13 and 3.63 Å that are in a good agreement with (002) and (110) plane of the orthorhombic crystalline structure of $Ta_3N_5$.

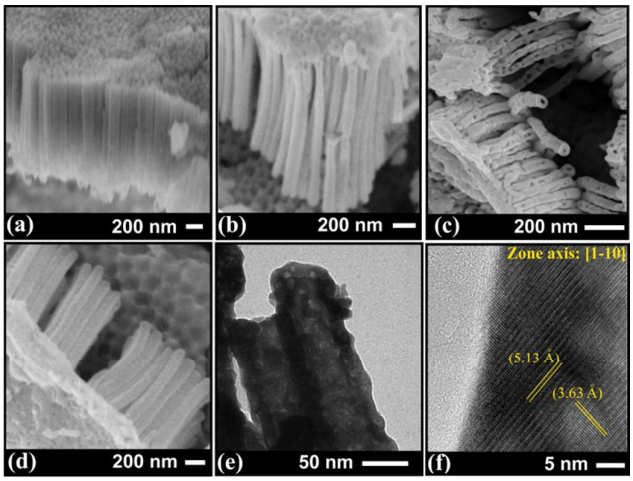


**Fig. 2** SEM images of (a) 800°C-5h, the samples prepared at (b) 850°C, (c) 1000°C and (d) 900°C for nitridation time of 3 hours. TEM (e) and HRTEM (f) images of 900°C-3h.

Hereafter, we will discuss the structural characterization for the samples that preserved tubular morphology; however, for comparison the PEC performances of all synthesized samples have been studied.

**Crystalline structure of $Ta_3N_5$ nanotubes**

Studying the crystalline structure of $Ta_3N_5$ NTs adhere to the Ta substrate by XRD is a challenge task as the Ta foil presents plastic deformation. The characteristic peaks of Ta substrate present high intensity thereby $Ta_3N_5$ peaks are hardly seen in the diffractogram. From the XRD patterns recorded by three different approaches; we have provided a comprehensive methodology to study this system (**Fig. 3)**. For comparison, the XRD of the precursor $Ta_2O_5$ is displayed in **Fig. 3a.** Only the diffraction peaks characteristic of Ta can be observed as expected; since the as–anodized $Ta_2O_5$ NTs are amorphous.[14] After thermal nitridation; the grey colored $Ta_2O_5$ NTs turned into red colored $Ta_3N_5$ NTs.[9] To investigate the presence of $Ta_3N_5$ phase we firstly performed conventional XRD of the NTs adhered to the Ta substrate (**Fig. 3b**). One can observe three different species in the samples; $Ta_3N_5$ (PDF# 79-1533), sub–nitride $TaN_{0.1}$ (PDF# 25-1278) and Ta (PDF# 4-788); their corresponding peaks are marked as *, Δ and Θ; respectively. In addition, the relative intensity of $TaN_{0.1}$ peaks increases with the temperature suggesting the increase in the concentration of sub–nitride phases at higher temperatures (**Fig. 3b**).[17] The presence of sub–nitride phase has been earlier reported;[9] however, no information is available on the location where it lies in the sample neither on how this phase is formed.

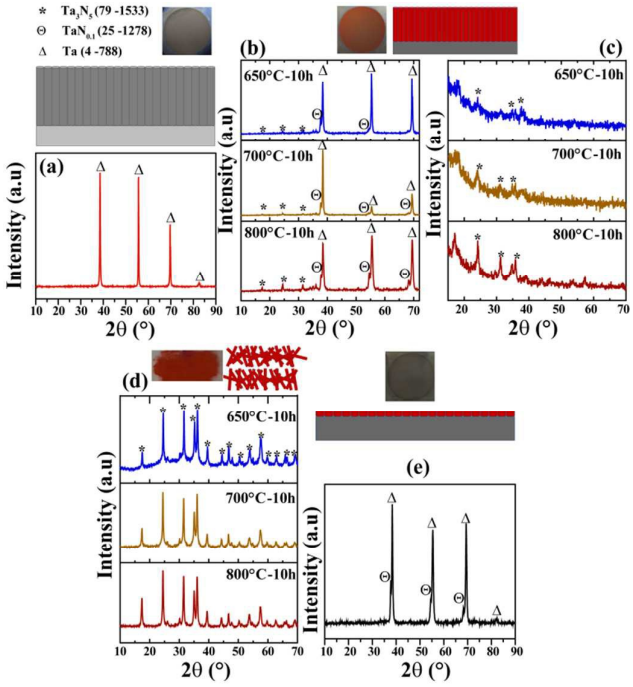


**Fig. 3** XRD patterns of (a) as-anodized $Ta_2O_5$ NTs/Ta, (b) and (c) $Ta_3N_5$ NTs/Ta, (d) $Ta_3N_5$ NTs removed from the substrate and (e) the substrate of which the $Ta_3N_5$ NTs are scratched off.

The SEM images in **Fig. 1 and 2** show that $Ta_3N_5$ NTs present a vertically oriented porous structure, allowing the $NH_3$ to diffuse from top to bottom to readily replace oxygen by nitrogen resulting in $Ta_3N_5$ NTs over the entire nanotube. It has been earlier observed that for the NTs of $Ta_3N_5$ the oxygen diffuses to the walls of the NTs and higher temperature nitridation decreases oxygen content.[11] Furthermore, according to the literature, pristine tantalum metal cannot readily react under flowing ammonia to form any nitride of tantalum (*XRD patterns of pure Ta before and after nitridation under flowing ammonia for high temperatures were exactly the same*).[18] Therefore, we suggest that the oxygen content that diffuses to the bottom Ta substrate reacts with the Ta atoms

forming non–stoichiometric oxides which then react with the $NH_3$ to transform into $TaN_{0.1}$. The Ta and $TaN_{0.1}$ peaks have higher relative intensity compared to $Ta_3N_5$ phase; therefore, a complete characteristic diffractograms for the whole $2\vartheta$ range of $Ta_3N_5$ could not be observed, instead; $Ta_3N_5$ peaks are visible up to $2\vartheta$ ~36°. In order to remove the substrate contribution, we have obtained the grazing angle XRD diffractograms of the nanotubes at a very small grazing angle of 0.3° (**Fig. 3c**). The substrate contributions are almost completely removed and the subnitride $TaN_{0.1}$ (present in conventional XRD) is absent in the grazing angle XRD, showing that $TaN_{0.1}$ is in fact a substrate contribution. In addition, for 650°C-10h the $Ta_3N_5$ peaks visible in **Fig. 3b** are nearly absent in **Fig. 3c** that shows the presence of $Ta_3N_5$ crystalline grains in amorphous $Ta_2O_5$ tubular matrix. Grazing angle XRD helped to minimize the contribution from the Ta substrate, however; at the same instant the signal resolution from $Ta_3N_5$ NTs have been lost. Hence, the NTs were removed from the Ta substrate and powder XRD diffractograms have been obtained for the scratched off NTs (**Fig. 3d**).[17] The signal resolution is highly improved and all of the observed peaks correspond to $Ta_3N_5$. Finally, XRD patterns obtained from the substrate of which the NTs were removed have shown just the $TaN_{0.1}$ and Ta characteristic peaks (**Fig. 3e**) strongly confirming the presence of $TaN_{0.1}$ at the substrate. Nevertheless, we found that $TaN_{0.1}$ is metallic; however, we suggest developing a certain strategy helping to avoiding these phases to synthesize $Ta_3N_5$ NTs for PEC applications.

With the aim to study pristine $Ta_3N_5$ NTs free from any other contribution from now onward we will discuss the XRD patterns obtained from the scratched off powders. To investigate the minimum nitridation conditions to obtain $Ta_3N_5$ NTs we started thermal nitridation at 650 °C for 1 h and 3 h. However, at these conditions the presence of a mixed structure of $Ta_2O_5$ (PDF# 25-922) and $Ta_3N_5$ (PDF# 79-1533) was observed (**Fig. S1**) and by increasing the nitridation time from 3h to 6h at 650°C (**Fig. S1**), clear changes in the XRD patterns are observed once pristine $Ta_3N_5$ phase is obtained at these conditions. Nevertheless, for 650°C-6h one can observe a huge background in the spectrum along with wide diffraction patterns presenting amorphism in the sample. Therefore, to further improve the crystallinity, we have increased the nitridation time to 10 h at 650°C (**Fig. 3d)**. The diffraction peaks are sharper when compared to 650°C-6 h (**Fig. S1)**; therefore, we fixed the nitridation time for 10 h and varied the temperatures to 700°C, 750°C, 800°C and 900°C**.** Furthermore, impurities were observed for 800°C-1h (**Fig. S1)**; and by increasing the time to 2 h at 800°C pristine $Ta_3N_5$ NTs are obtained. **Fig. 4** displays the XRD patterns of phase-pure orthorhombic $Ta_3N_{5\ NTs}$ corresponding to the PDF# 79-1533. Interestingly, when compared to commercial $Ta_2O_5$ powders which are crystalline in nature, the transformation from $Ta_2O_5$ NTs to $Ta_3N_5$ NTs is found to take place at a lower temperature of 650°C.[16] We may suggest that amorphous nanotubular precursors of $Ta_2O_5$ are easy to transform to $Ta_3N_5$ at low temperature.

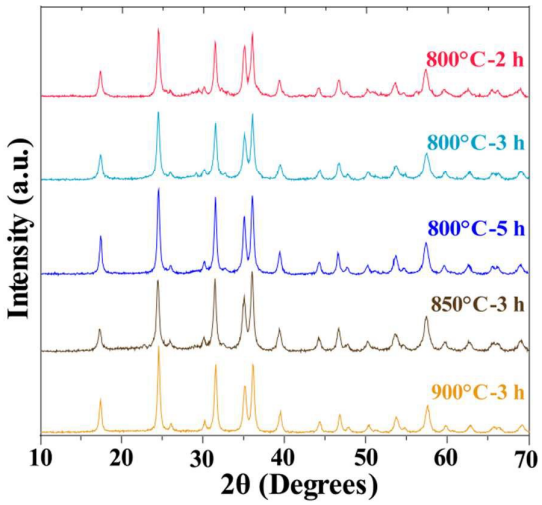


**Fig. 4** XRD patterns of $Ta_3N_5$ NTs prepared by thermal nitridation.

Crystalline structures were refined by the Rietveld technique. Simulated patterns (**Fig. S2**) and their respective parameters are shown in **Table 1** and **Table S2.** For the set of samples prepared for 10 h, in addition to slight increase in the grain size the strain is increasing with the temperature (**Table 1)**. The increase in the strain might be related to the morphology preservation and increasing the roughness on the walls of the NTs. The larger crystalline grains and improved crystallinity were obtained for the 900°C-3h $Ta_3N_5$ NTs. Unlike earlier report on $Ta_3N_5$ thin films, the grain size for $Ta_3N_5$ NTs found here presents a dependence on the nitridation conditions.[19] This behavior can be rationalized on the basis of different crystal growth phenomena for thin films and tubular morphology. Once thin films are compact and during the crystal growth; the grains exhibit stress from their neighbor grains that may limit their further growth due to the compact nature of thin films. Therefore, within the limit of stability of $Ta_3N_5$ phase the grains become independent of the nitridation temperature.[19]

**Table 1**. Grain size, lattice strain and nominal stoichiometries obtained from the refinements for $Ta_3N_5$ NTs.

| Sample | Av. Grain Size (nm) | Strain($\times10^{-4}$) | Stoichiometry |
|---|---|---|---|
| 650°C-10h | 29.59 | 12.15 | $Ta_{2.97}N_{2.71}O_{2.0}$ |
| 700°C-10h | 32.56 | 19.93 | $Ta_{2.94}N_{3.43}O_{1.25}$ |
| 800°C-5h | 31.53 | 18.67 | $Ta_{2.90}N_{4.26}O_{0.67}$ |
| 800°C-10h | 37.46 | 22.00 | $Ta_{2.91}N_{4.55}O_{0.39}$ |
| 850°C-3h | 34.03 | 32.43 | $Ta_{2.98}N_{4.29}O_{0.48}$ |
| 900°C-3h | 43.51 | 36.90 | $Ta_{2.99}N_{4.61}O_{0.22}$ |

On the other hand, NTs are isolated from their surrounding exhibiting lower stress from the neighboring grains during the growth; thereby, high temperature nitridation facilitates to increase their size. However, care must be taken for tubular morphology once the morphology can be collapsed under very harsh nitridation conditions.

The percentages of defects in the crystalline structure of $Ta_3N_5$ NTs are calculated considering the occupation factors obtained by

Rietveld refinement (**Table S2**). At the Wyckoff sites Ta1(4c), Ta2(8f) and N1(8f) Schottky defects were found. Following the methodology proposed by Henderson et al,[20] the refinements were improved when oxygen substitutional defects are incorporated at the 3-coordinated Wyckoff site N2(4f). These results confirm that oxygen in the crystalline structure of $Ta_3N_5$ cannot be completely removed by thermal nitridation.[20,21] Based on the refinements, nominal stoichiometries of the samples were calculated from the percentages of site occupancy and vacancy (**Table S2**) that were obtained from the occupation factors; and are displayed in **Table 1**. In the set of samples prepared for the nitridation of 10 h, one can observe a decrease in oxygen content by increasing the temperature. However, for 650°C-10h the Ta stoichiometry is "2.94" i.e greater than the other samples but oxygen content are highest; suggesting the presence of large oxygen content in the sample. Therefore, we may suggest; for sample 650°C-10h, the $Ta_3N_5$ crystalline grains are distributed in the amorphous tubular matrix of $Ta_2O_5$. In addition, the stoichiometry was not ideal even for 800°C-10h. These results strongly suggest that indeed nitridation temperature of 800°C is not an optimum condition for the synthesis of $Ta_3N_5$.[9,15] Therefore, the temperature should be increased; however care must be taken to choose an appropriate nitridation time, in order to preserve the tubular morphology. Further details on the crystalline structure of the samples prepared for 3 h of nitridation as a function of nitridation temperature are discussed elsewhere.[11]

Surface elemental composition was investigated by XPS; for the sake of comparison 800°-10 h and 900°C-3 h were chosen for the analyses. From the survey spectra (not shown) characteristic peaks of Ta, N, O and C were observed. **Fig. 5** displays the high resolution XPS spectra of Ta4f and N1s peaks. For both of the samples; in Ta4f region the $Ta4f_{7/2}$ and $Ta4f_{5/2}$ doublet are centered at 24.6 and 26.5 eV, respectively with a spin orbital splitting of 1.9 eV. These positions are in line with $Ta^{5+}$ of $Ta_3N_5$. Furthermore, N1s is positioned at 396.2 eV. These energies are consistent with the previously reported positions observed for $Ta_3N_5$.[9,22]

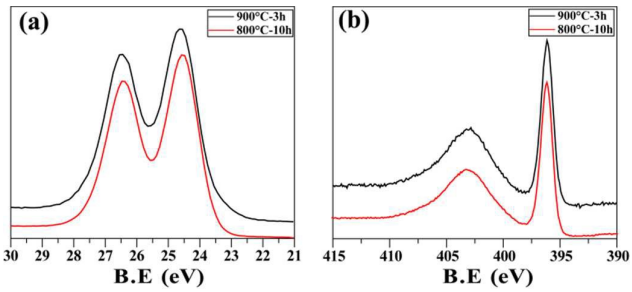


**Fig. 5.** High resolution XPS spectra of (a) Ta4f and (b) N1s region of $Ta_3N_5$ NTs. In N1s region the peak at ca. 403 eV is attributed to $Ta4p_{3/2}$.

### Optical characterization

After nitridation a red color was visually observed for the samples indicating the formation of $Ta_3N_5$ NTs.[22,23] **Fig. 6** displays the UV–Vis diffuse reflectance spectra of $Ta_2O_5$ and some selected samples of $Ta_3N_5$ NTs. The absorption edges of the $Ta_3N_5$ have been red shifted from the $Ta_2O_5$ edge due to narrowing of the band gap. The direct and indirect band gaps were obtained by extrapolating the linear region on the UV-Vis spectra and were found to ca. 2.1–2.2 and 1.93–1.98 eV, respectively consistent with the reported values for $Ta_3N_5$.[9,16] The absorption spectra of all samples presented tails in ca. 600– 800 that has been attributed to the ionic defects.[24]

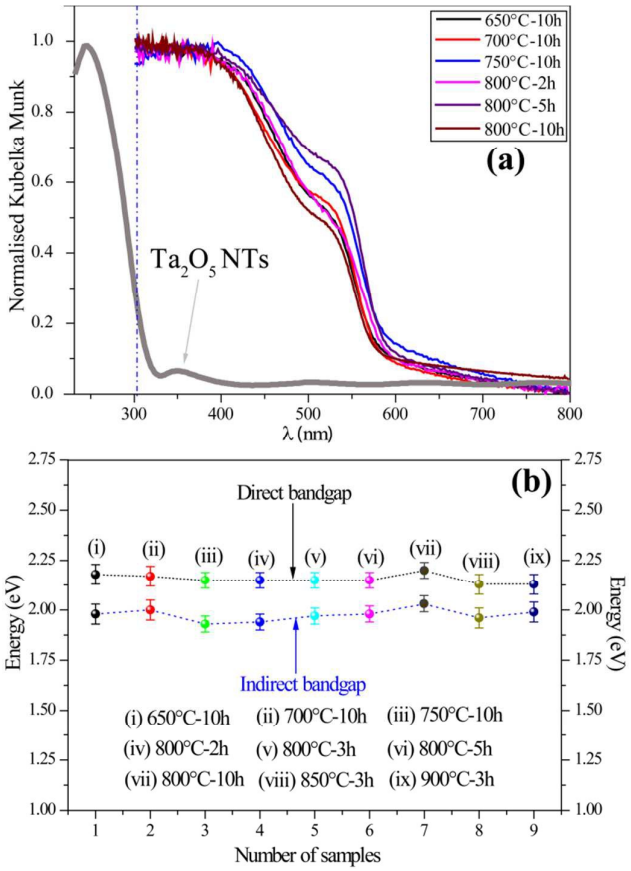


**Fig. 6.** (a) Absorption spectra and (b) direct bandgap obtained from *[K.M (R)hv]* $^2$ vs *hv* and indirect bandgap obtained from *[K.M (R)hv]*$^{0.5}$ vs *hv* for $Ta_3N_5$ NTs.

### Electrochemical impedance spectroscopy (EIS)

To investigate the effect of nitridation conditions on the charge transfer across the $Ta_3N_5$ NTs–electrolyte interface, we have performed EIS (**Fig. 7**). Prior to the measurements; the samples were cleaned by successive cyclic voltammetry runs. For the set of samples prepared for the nitridation time of 10 h (**Fig. 7a**); incomplete semicircles can be observed which are characteristic of capacitance systems exhibiting non ideal behavior. As observed in the TEM images displayed in **Fig. 1 (bottom),** nitridation for longer time at high temperatures results in a rougher structure, which can affect the charge transportation at the interface. From the single semicircles (one time constant) shown in the **Fig. 7a** EIS data was fitted to an equivalent circuit (**Fig. 7d**); consisting of a series resistance $R_s$ and single CPE (constant phase element) parallel with

charge transfer $R_{ct}$. The CPE in an electrochemical system may arise from: (a) distribution of the relaxation times due to non-homogeneities existing at the electrode– electrolyte interface, (b) porosity of the electrode, (c) the nature of the electrode and (d) dynamic disorder associated with diffusion.[25,26,27]

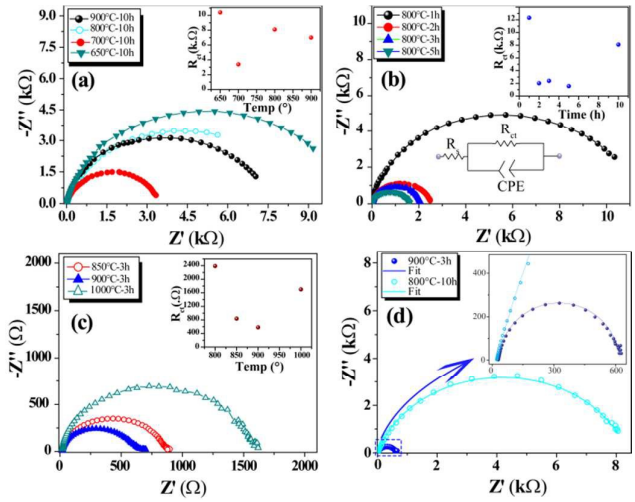


**Fig. 7** Nyquist plots for $Ta_3N_5$ NTs prepared at different nitridation conditions; obtained under dark (a, b and c) and AM 1.5 (1 Sun) illumination (d).

Therefore, based on the nanotubular nature and structural non-homogeneities (SEM and Rietveld refinements) adding CPE for the $Ta_3N_5$ NTs–electrolyte interface is physically true. By fitting the Nyquist plots into the proposed equivalent circuit the values of the components have been found and to better visualize the $R_{ct}$ as a function of various nitridation temperatures and times; we have plotted $R_{ct}$ against different thermal treatments shown in the inset of Nyquist plots in **Fig. 7**. The 650°C-10h sample presents the highest $R_{ct}$ (**Fig. 7a**). In the XRD patterns of the sample some amorphism was observed (**Fig. 3d**) and as observed in the Rietveld refinements (**Table 1**), the sample consists of highest oxygen content. Therefore, it is reasonable to propose that the amorphism and the highest oxygen content in the sample are the main reasons for the highest $R_{ct}$. Interestingly, 700°C-10h has exhibited the lowest $R_{ct}$. The stoichiometry of both 650°C-10h and 700°C-10h samples (**Table 1)** show the presence of oxygen content and 700°C-10h is more crystalline than 650°C-10 and present a small $R_{ct}$. Also 800°C-10h present slightly higher $R_{ct}$ compared to 900°C-10h, which might be related to smaller concentration of defects as can be inferred from the stoichiometry of $Ta_{2.99}N_{4.61}O_{0.22}$ obtained for sample prepared at 3h of nitridation time at 900° i.e 900°C-3h (**Table 1**). Now evaluating the samples prepared at fixed temperature of 800°C and varying nitridation times (**Fig. 7b);** 800°C-1h (consisting of mixed phases of $Ta_3N_5$ and $Ta_2O_5$ as shown in **Fig. S1**) present the highest $R_{ct}$ while 800°C-5h presents the smallest $R_{ct}$. Lastly, for the set of 3h samples (**Fig. 7c**), 900°C-3h evidently indicates the lowest interfacial charge transfer resistance compared to all of the samples synthesized in the current work corroborating the high crystallinity and phase purity as discussed earlier (**Table 1**). These results strongly suggest that nitridation conditions alter the crystalline structure of $Ta_3N_5$ NTs that further affects the interfacial charge transportation properties that are the functions of morphology, crystallinity and phase purity of $Ta_3N_5$ NTs photoanodes and for the lowest $R_{ct}$ an optimum is exhibited for 900°C-3h.

The samples prepared during short and long nitridation times were further probed by EIS, under illumination (**Fig. 7d)**. One can observe that both samples present a decrease in $R_{ct}$. Under illumination the photogenerated charge carriers are separated, thereby facilitating hole transfer from the semiconductor to the electrolyte, which results in a decrease of $R_{ct}$. In addition, 900°C-3h present lower $R_{ct}$ than 800°C-10h, under both conditions (dark and illumination). These results suggest that the sample prepared during longer nitridation exhibit a slower charge transfer at semiconductor–electrolyte interface.

**Mott-Shottky plots**

The flat band potential of the semiconductor is one of the most important parameters for evaluating photoelectrochemical water splitting, which help to predict whether semiconductor should be biased externally or not. One of the most widely used technique to estimate the flat band of a semiconductor is the Mott-Shottky plot.[28] **Fig. 8** displays the Mott-Shottky plots of the $Ta_3N_5$ NTs that present n-type transition from the positive slopes of the curves. On each graph the flat band potential ($E_{fb}$) is obtained by extrapolating the linear region which is presented as blue line intercepts. A very interesting result is that all of the samples present almost the same flat band potential of ca. –0.05 vs RHE; therefore, for $Ta_3N_5$ NTs, the $E_{fb}$ is almost independent of nitridation temperature. In addition, samples 650°C-10h and 700°C-10h present a lower transition along with the main transition (highlighted in **Fig. 8**); that can be related to the presence of oxide content which are higher in 650°-10h than in 700°-10h.

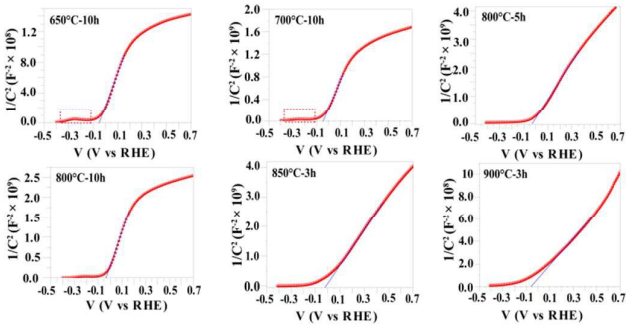


**Fig. 8** Mott-Schottky plots of $Ta_3N_5$ NTs synthesized at various nitridation conditions.

**PEC activity of $Ta_3N_5$ NTs**

**Fig. 9** shows the Linear Sweep voltammetry (LSV) curves of all the samples. Among the set of samples prepared for 10h of nitridation, 650°C-10h has presented lowest PEC activity which can be related to lower order crystallinity (**Fig. 3c**) as well as highest interfacial $R_{ct}$

(**Fig. 7a**). On the other hand the highest photocurrent was obtained from 900°C-10h that can be related to the improved stoichiometry of the sample obtained at 900°C compared to the samples prepared at 800°C (**Table 1**). For the set of samples prepared at fixed temperature of 800°C by varying nitridation time (**Fig. 9b**); the sample 800°C-1h has shown poor PEC performance. The XRD analysis presents the mixture of $Ta_2O_5$ and $Ta_3N_5$ phases for 800°C-1h (**Fig. S1**). The trade-off between the sample chemical composition and the electrolyte clearly influences the PEC performance. Therefore, the impure phase and low crystallinity are the main reasons behind the poor performance of 800°C-1h. Interestingly 800°C-5h presented the higher PEC activity even compared to 800°C-10h. This result can be related to the thermal decomposition of the $Ta_3N_5$ at longer nitridation periods.[24] Although, 800°C-5h presents the higher photocurrent compared to other samples of the set; however, the photocurrent is still low, which can be rationalized in terms of the stoichiometries of the samples prepared at 800°C for varying nitridation times i.e, which are far away from the ideal $Ta_3N_5$ (**Table 1**). Therefore, 800°C is not a good choice to synthesize $Ta_3N_5$ NTs. Considering now the nitridation of the samples for fixed time of 3h under varying temperatures; clearly the 900°C-3h presented improved photocurrent compared to all other samples prepared in the current work and to those shown in the earlier reports.[15,29] In addition, the photocurrent from 900°C-3h [11] is nearly 2–3 fold more than that obtained from 900°C-10h and 1000°C-3h. Therefore, the improved photocurrent from $Ta_3N_5$ nanotubular photoanodes is in fact a synergistic combination of the tubular morphology, the controlled chemical composition and the improved charge transfer across the interface.

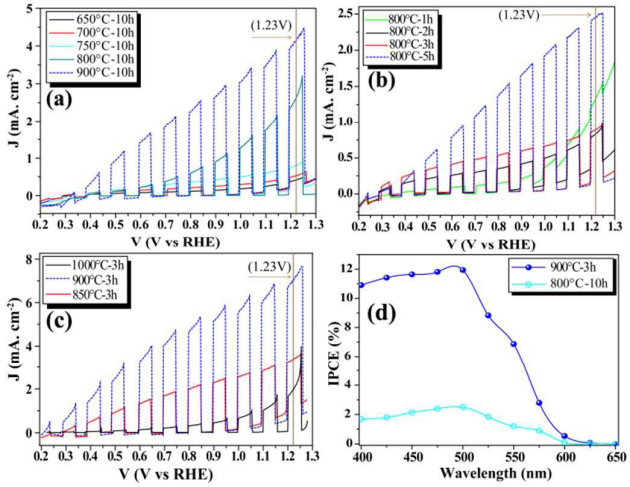


**Fig. 9** LSV curves (a, b & c) obtained by chopping AM 1.5 (1 Sun) illumination and IPCE spectra (d) of $Ta_3N_5$ NTs.

**Table. S3** shows the parameters obtained from LSV experiments. The $V_{oc}$ values for pristine $Ta_3N_5$ NTs are found nearly independent of the nitridation conditions. This behavior might be related to the position of the flat band that was found to be the same for pristine $Ta_3N_5$ NTs, however, 800°C-1h presented a slightly different $V_{oc}$; related to the presence of impurities in the sample.

**Fig. 9d** shows the incident photon-to-current conversion efficiency (IPCE) for the samples obtained after short and long nitridation periods. The IPCE was calculated by the following equation:

$$IPCE(\%) = 1240 \times (J_{ph}/\lambda P_{in}) \times 100$$

where $J_{ph}$ is the photocurrent (in A/m$^2$), $\lambda$ is the wavelength (in nm) of incident radiation, and $P_{in}$ is the incident light power intensity (in W/m$^2$) on the semiconductor photoelectrode at the given wavelength. For both samples the IPCE presents a maximum at 500 nm that was 11.8% for 900°Ch-3h and 2.5% for 800°C-10h, which corroborates the photocurrent obtained from these samples. Furthermore, IPCE spectra follow the same trend as that of UV-Vis absorbance of the samples (**Fig. 6**), and also comparable to the literature.[15]

## Conclusions

In summary, we have performed a throughout study on the effect of nitridation temperature and time on the syntheses of $Ta_3N_5$ NTs by thermal nitridation of the anodized precursor $Ta_2O_5$ NTs. We observed that amorphous $Ta_2O_5$ NTs are easier to transform to $Ta_3N_5$ by nitridation at low temperatures; however the samples obtained at lower temperatures present low crystallinity and poor photoelectrochemical performance. To synthesize $Ta_3N_5$ NTs by thermal nitridation; the temperature should be high enough to obtain higher crystallinity and the nitridation time should be short enough to preserve the tubular morphology. The combined effect of high crystallinity, tubular morphology and low charge transfer resistance across $Ta_3N_5$ NTs-electrolyte interface presents an optimized nitridation condition. Based on Rietveld refinement, EIS and LSV curves the sample 900°C-3h presents optimum features of a promising photoelectrode prepared in the current study.

## Acknowledgements

The authors are grateful for financial support from the following Brazilian agencies: Conselho Nacional de Desenvolvimento Científico e Tecnológico (Processo: 477804/2011-0, 490221/2012-2 and 472243/2013-6) and Fundação de Amparo à Pesquisa do Estado do Rio Grande do Sul (FAPERGS – PqG 2011 Proc. 11/0837-0). Thanks are due to MSc. Maximiliano J. M. Zapata for help in Rietveld Refinements, Dr. Daniel Baptista for HRTEM image and Mr. Andre Vargas from PUCRs-POA, Brazil for performing grazing angle XRD.

## References

1. Y. Li, L. Zhang, A. Torres-Pardo, J. M. Gonzalez-Calbet, Y. Ma, P. Oleynikov, O. Terasaki, S. Asahina, M. Shima, D. Cha, L. Zhao, K. Takanabe, J. Kubota and K. Domen, *Nat. Commun.*, 2013, **4**, 1.

2. R. G. Sabat, M. J. L. Santos and P. Rochon, *Int. J. Photoenergy*, 2010, **2010**, 5.
3. M. J. L. Santos, A. F. Rubira, R. M. Pontes, E. A. Basso and E. M. Girotto, *J. Solid State Electrochem.*, 2006, **10**, 117.
4. J. A. Fernandes, P. Migowski, Z. Fabrim, A. F. Feil, G. Rosa, S. Khan, G. J. Machado, P. F. P. Fichtner, S. R. Teixeira, M. J. L. Santos and J. Dupont, *Phys. Chem. Chem. Phys.*, 2014, **16**, 9148.
5. S. Khan, M. J. M. Zapata, M. B. Pereira, R. V. Goncalves, L. Strizik, J. Dupont, M. J. L. Santos and S. R. Teixeira, *Phys. Chem. Chem. Phys.*, 2015 **17** 23952.
6. P. Zhang, T. Wang, J. Zhang, X. Chang and J. Gong, *Nanoscale*, 2015, **7**, 13153.
7. K. Maeda, N. Nishimura and K. Domen, *Appl. Catal. A-Gen.*, 2009, **370**, 88.
8. X. J. Feng, T. J. LaTempa, J. I. Basham, G. K. Mor, O. K. Varghese and C. A. Grimes, *Nano Lett.*, 2010, **10**, 948.
9. Y. Cong, H. S. Park, S. Wang, H. X. Dang, F.-R. F. Fan, C. B. Mullins and A. J. Bard, *J. Phys. Chem. C*, 2012, **116**, 14541.
10. L. Wang, N. T. Nguyen, X. Zhou, I. Hwang, M. S. Killian and P. Schmuki, *ChemSusChem*, 2015, (Doi:10.1002/cssc.201500632).
11. S. Khan, M. J. M. Zapata, D. L. Baptista, R. V. Gonçalves, J. A. Fernandes, J. Dupont, M. J. L. Santos and S. R. Teixeira, *The J. Phys. Chem. C*, 2015 (DOI: 10.1021/acs.jpcc.5b05475).
12. B. Klahr, S. Gimenez, F. Fabregat-Santiago, J. Bisquert and T. W. Hamann, *Energ. Environ. Sci.*, 2012, **5**, 7626.
13. J. G. Hou, Z. Wang, C. Yang, H. J. Cheng, S. Q. Jiao and H. M. Zhu, *Energ. Environ. Sci.*, 2013, **6**, 3322.
14. Y. Kado, C. Y. Lee, K. Lee, J. Muller, M. Moll, E. Spiecker and P. Schmuki, *Chem. Comm.*, 2012, **48**, 8685.
15. Q. H. Zhang and L. Gao, *Langmuir*, 2004, **20**, 9821.
16. R. V. Goncalves, P. Migowski, H. Wender, A. F. Feil, M. J. M. Zapata, S. Khan, F. Bernardi, G. M. Azevedo and S. R. Teixeira, *CrystEngComm*, 2014, **16**, 797.
17. Y. B. Li, T. Takata, D. Cha, K. Takanabe, T. Minegishi, J. Kubota and K. Domen, *Adv. Mater.*, 2013, **25**, 125.
18. M. Hara, E. Chiba, A. Ishikawa, T. Takata, J. N. Kondo and K. Domen, *J. Phys. Chem. B*, 2003, **107**, 13441.
19. B. A. Pinaud, A. Vailionis and T. F. Jaramillo, *Chem. Mater.*, 2014, **26**, 1576.
20. S. J. Henderson and A. L. Hector, *J. Solid State Chemi.*, 2006, **179**, 3518.
21. J. Wang, J. Feng, L. Zhang, Z. Li and Z. Zou, *Phys. Chem. Chem. Phys.*, 2014, **16**, 15375.
22. W. J. Chun, A. Ishikawa, H. Fujisawa, T. Takata, J. N. Kondo, M. Hara, M. Kawai, Y. Matsumoto and K. Domen, *J. Phys. Chem. B*, 2003, **107**, 1798.
23. C. M. Fang, E. Orhan, G. A. de Wijs, H. T. Hintzen, R. A. de Groot, R. Marchand, J. Y. Saillard and G. de With, *J. Mater. Chem.*, 2001, **11**, 1248.
24. A. Dabirian and R. van de Krol, *Appl. Phys. Lett.*, 2013, **102** 033905.
25. D. P. Dubal, S. H. Lee, J. G. Kim, W. B. Kim and C. D. Lokhande, *J. Mater. Chem.*, 2012, **22**, 3044.
26. J.-B. Jorcin, M. E. Orazem, N. Pébère and B. Tribollet, *Electrochim. Acta*, 2006, **51**, 1473.
27. M. R. Shoar Abouzari, F. Berkemeier, G. Schmitz and D. Wilmer, *Solid State Ionics*, 2009, **180**, 922.
28. L. Djellal, A. Bouguelia and M. Trari, *Mater. Chem. Phys.*, 2008, **109**, 99.
29. D. Yokoyama, H. Hashiguchi, K. Maeda, T. Minegishi, T. Takata, R. Abe, J. Kubota and K. Domen, *Thin Solid Films*, 2011, **519**, 2087.

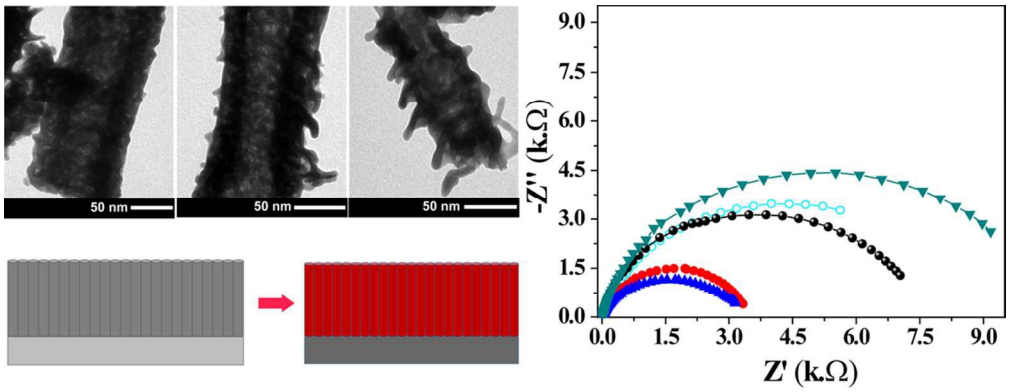


97x37mm (300 x 300 DPI)